RESEARCH ARTICLE

A high-resolution outgoing longwave radiation dataset from Kalpana-1 satellite during 2004–2012

M. Mahakur[1,*], A. Prabhu[1], A. K. Sharma[2], V. R. Rao[2], S. Senroy[2], Randhir Singh[3] and B. N. Goswami[1]

[1]Indian Institute of Tropical Meteorology, Dr. Homi Bhabha Road, NCL Post, Pashan, Pune 411 008, India
[2]India Meteorological Department, Mausam Bhavan, Lodhi Road, New Delhi 110 003, India
[3]Atmospheric Sciences Division, AOSG/EPSA, Space Applications Centre, ISRO, Ahmedabad 380 058, India

Long record of high-resolution quality-controlled outgoing longwave radiation (OLR) from geostationary platforms like Kalpana-1 has the potential not only to provide detailed information of cloud types contributing to the measure of rain, but also helps unravel convective cloud organization in the tropics from small scale to meso- and synoptic scales. A research quality product of three hourly OLR for the period May 2004–June 2012 is produced from Kalpana-1 very high resolution radiometer (VHRR) radiances over the Indian region (40°S–40°N, 25–125°E) in a regular grid of 0.25 × 0.25 degrees. The quality and usefulness of the dataset is demonstrated here using some illustrative examples. Although these data are available for a relatively short-period, it is shown that they will be potentially more useful than the widely used OLR from NOAA satellites in representing the annual cycles, particularly over the desert and humid oceans, due to their frequent sampling and quality. The active–break periods in the Indian summer monsoon picked up by both the OLR match well. This three hourly OLR estimated from Kalpana-1 VHRR is able to describe the fine-scale structure of the diurnal variation over the region.

Keywords: Active–break periods, diurnal variation, geostationary platforms, outgoing longwave radiation.

OUTGOING longwave radiation (OLR) is the radiant energy or the radiative flux leaving the Earth–atmosphere system in the infrared (IR) region of the electromagnetic spectrum in a very broad wavelength ranging from 4 to 100 μm. It is an important component in the Earth's total energy budget. OLR is sensitive to clouds and water vapour and to some extent to dust and other greenhouse gases in the atmosphere. The surface and vertical distribution of temperature and therefore the circulation of the atmosphere is decided depending upon the difference between the net incoming solar radiation and OLR. The estimation of planetary radiation budget by satellites started since the beginning of the environmental satellite programme in early 1960s, but was for limited periods depending upon the lifetime of those experimental satellites[1]. Although somewhat longer direct measurement of the broadband radiation budget began with the launch of Nimbus 6 and 7, the operationally available longest series of satellite estimations of OLR started from the NOAA series of satellites[2,3] during early 1970s. OLR is widely used as a tool in numerous applications such as climate sensitivity and diagnosis[4–8], weather and climate predictions[9–11], studies on monsoon variability[12–14] and equatorial waves[15–19]. OLR is considered as a proxy for the deep convection and used for precipitation estimation[20–22].

Long continuous OLR data with high resolution in both space and time are not available over the Indian region from any Indian satellite to provide a better definition of diurnal variability and for representation of the small-scale variability due to inhomogeneous surface type and/or organization of convective cloud systems. The high-impact weather event which generally occurs from deep convective clouds, is small in spatial and temporal scales present within the large-scale environment. The interactions of both these scales are crucial in the understanding of such weather events. Therefore, an effort has been made to estimate OLR at every three hourly basis (i.e. at 00 UTC, 03 UTC, etc.) with a spatial resolution of 0.25 × 0.25 degrees from the observed radiances of Kalpana-1 VHRR (very high resolution radiometer), archived at the National Satellite Data Centre, India Meteorological Department, New Delhi. This article describes the estimation of OLR data and demonstrates its potential utilities in some areas like annual, intra-seasonal and diurnal variability. These estimated high-resolution OLR data will be made available to the users.

Kalpana-1 (formerly METSAT-1) is India's first dedicated meteorological satellite with initial mission life of seven years; stationed at 74°E, it was launched on 12 September 2002 for the first time using polar satellite launch vehicle (PSLV) into the geostationary orbit. The satellite payloads consist of a data relay transponder (DRT) and VHRR for meteorological applications. The

*For correspondence. (e-mail: mmahakur@tropmet.res.in)

main instrument of Kalpana-1 is the VHRR for imaging in three spectral bands namely VIS (visible; 0.55–0.75 μm), thermal IR (10.5–12.5 μm) and WV (water vapour; 5.7–7.1 μm)[23]. The VIS and IR channels are within the atmospheric windows, whereas the WV channel (centred at 6.2 μm) is sensitive to moisture content in the mid–upper troposphere of the atmosphere with weighting function peaks around 400 hPa (ref. 24). The nominal spatial resolution (i.e. pixel size) of images obtained by these three channels for a nadir-viewing scan position is 2, 8 and 8 km respectively, which is an improvement upon the first generation of the INSAT (Indian national satellite) series[23].

Estimation of OLR from IR and WV radiances of Kalpana-1 VHRR

OLR is measured somewhat directly by broadband instruments such as Earth radiation budget experiment (ERBE), scanner radiometer for radiation budget (ScaRab), and clouds and Earth's radiant energy system (CERES). Some of the low Earth orbiting satellites such as Nimbus, ERBS (Earth radiation budget satellite), Aqua, TRMM (tropical rainfall measuring mission) were launched with one of these instruments. The ScaRab is also one of the payloads on-board the *Megha-Tropiques* satellite launched on 12 October 2011, which is a joint Indo-French mission for studying the hydrological cycle over the tropics. The long-term routinely available OLR is being estimated by converting the narrow band thermal IR (10–12 μm) observed radiances into the broadband (4–100 μm) flux[3,25], such as NOAA OLR[26,27]. These estimated OLR from the IR window channel equivalent blackbody temperatures employing empirical techniques such as linear regression, developed from the theoretical a priori radiative transfer calculations. This was also used in estimating OLR from INSAT[28] until now starting from the launch of the first-generation INSAT. However, the IR window channel is primarily sensitive to the temperature of the lowest visible surface (i.e. either land/ocean or cloud top), but the measured OLR at the top of the atmosphere is also sensitive to the vertical distribution of temperature and moisture. Subsequently, to improve the accuracy of the empirically estimated OLR more than one channel was used[29], by a suitable combination of imager and sounder channels. Hitherto none of the geostationary satellites has a broadband radiometer; therefore OLR is being obtained from the one or more available narrow-band channels. Further, the geostationary satellites have the advantage of making frequent sampling of OLR over the regions under their coverage and are not prone to bias like several NOAA satellites, due to drift in the local time of visit of their Sun-synchronous orbits. It has been shown[30] that the bias in the most popularly used NOAA OLR due to this orbital drift is as large as 12 Wm^{-2}. Further, as the diurnal cycle of the OLR is not symmetric between night and day, the available daily averages obtained from two observations separated by 12 h become more biased compared to that from true average. Therefore, OLR from geostationary satellites needs more emphasis with a better estimation using multiple channels of imager and sounder. However, till the launch of INSAT-3D (which will fly with sounder channels), one has to rely upon the VHRR on-board INSAT or Kalpana-1 satellite, by developing more accurate estimation algorithms such as the genetic algorithm (GA)[31].

Three hourly (at synoptic hours) OLRs from the IR and WV radiances have been estimated for the period May 2004–June 2012. From the image digital grey counts (10-bit resolution) radiances were obtained by matching with the corresponding look-up-table (LUT), which is generated on-board the satellite for every full scan. Prior to this conversion the images were checked for distortion in scan line and individual pixels due to radiometric noises or problems in telemetry were omitted while doing further calculations. Geo-location of the full disc images was done by performing 'near-sided perspective map projection' by utilizing satellite navigation information such as false easting and northing positions and satellite altitude[32]. Required correction to the shifting of the image due to problem in instrument orientation was also done while performing geo-locations of the image pixels.

OLR values are estimated for every geo-located pixel utilizing the empirical relations[31] between OLR and narrow-band IR and WV radiances as well as satellite zenith angle (up to 70°). These relations were developed for channels specific to Kalpana-1 from the theoretically modelled OLR using forward radiative transfer simulations for both cloudy as well as clear sky conditions[31]. GA is a widely used nonlinear optimization technique, suitable for small-sized samples as well. The root mean square error in the estimated OLR using the empirical equations suggested by GA[31] is below 3 Wm^{-2}, with negligible bias and is as accurate as that from NOAA HIRS (high-resolution infrared sounder) multichannel product[29]. Finally, the OLR values are obtained in regular grid bins of 0.25° × 0.25° over the geographical region 40°S–40°N, 25–125°E, at every synoptic hour (i.e. three hourly) by performing weighted (cosine of the latitude of the pixel) average of the all pixels in the grid boxes. The number of pixels within these grid boxes ranges from 12 near the sub-satellite points to around 2–3 pixels within a grid box at large zenith angles. During the estimation period (i.e. May 2004–June 2012) less than 20% of the imageries was found to be missing, but for 18 UTC the percentage was somewhat high. The large number of missing images at 18 UTC slot is due to lack of observations during the months when Earth is near the equinox (i.e. March–April and September–October) during the estimation period. This is due to the Sun being in the field-of-view as the satellite enters and leaves the Earth's

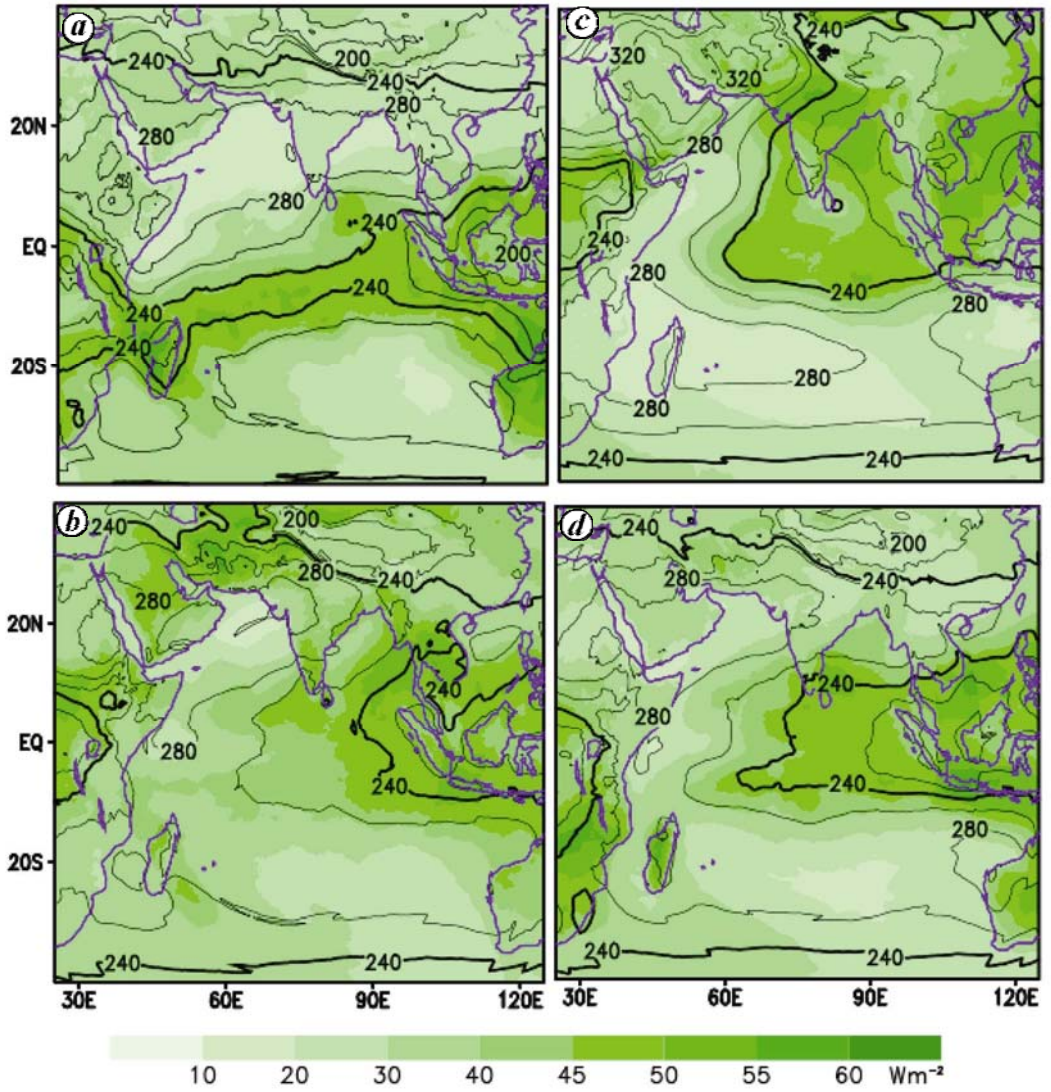

Figure 1. Seasonal average (contour lines) and standard deviation (shaded) of outgoing longwave radiation (OLR) during the period 2004–2012 obtained from Kalpana-1 three hourly observations. (***a***) Winter (January–February), (***b***) Pre-monsoon (March–May), (***c***) Monsoon (June–September) and (***d***) Post-monsoon (October–December) seasons. The 240 Wm^{-2} OLR values are highlighted with thick and dark contours.

shadow near 2300 and 0100 h local time and because INSAT and Kalpana being three-axis stabilized systems, the instrument is closed during this period to prevent direct Sun rays entering it. Although OLR was estimated for the above durations, for the analysis of annual cycles and monsoon intraseasonal variability only the data of January 2005 up to December 2011 were utilized.

Figure 1 shows average and standard deviation of the OLR for various climatological seasons, obtained from the three hourly Kalpana-1 data for 2004–2012. The standard deviation includes variation during the day and night over each location, since it is computed from the three hourly OLR values. It shows that the variability of the OLR at its maximum over the zone of convective maxima having average values less than 240 Wm^{-2}. The standard deviation is also equally high over the arid and semi-arid regions, where the amplitude of diurnal variations (shown later) is found to be very high.

Comparison of Kalpana-1 and NOAA OLR

The Kalpana-1 daily averaged OLR obtained by averaging all the three hourly values available in a day is compared with that obtained from NOAA OLR[26,27]. The NOAA OLR during this period is from NOAA-16 and NOAA-18 satellites, whose equatorial daytime of crossing is at 1350 h and 1355 h LST (local standard time) respectively; the night visit is after a gap of 12 h (http://www.esrl.noaa.gov/psd/data/gridded/data.interp_OLR.html). Here we choose to compare with the NOAA data because these are most widely used, and are also

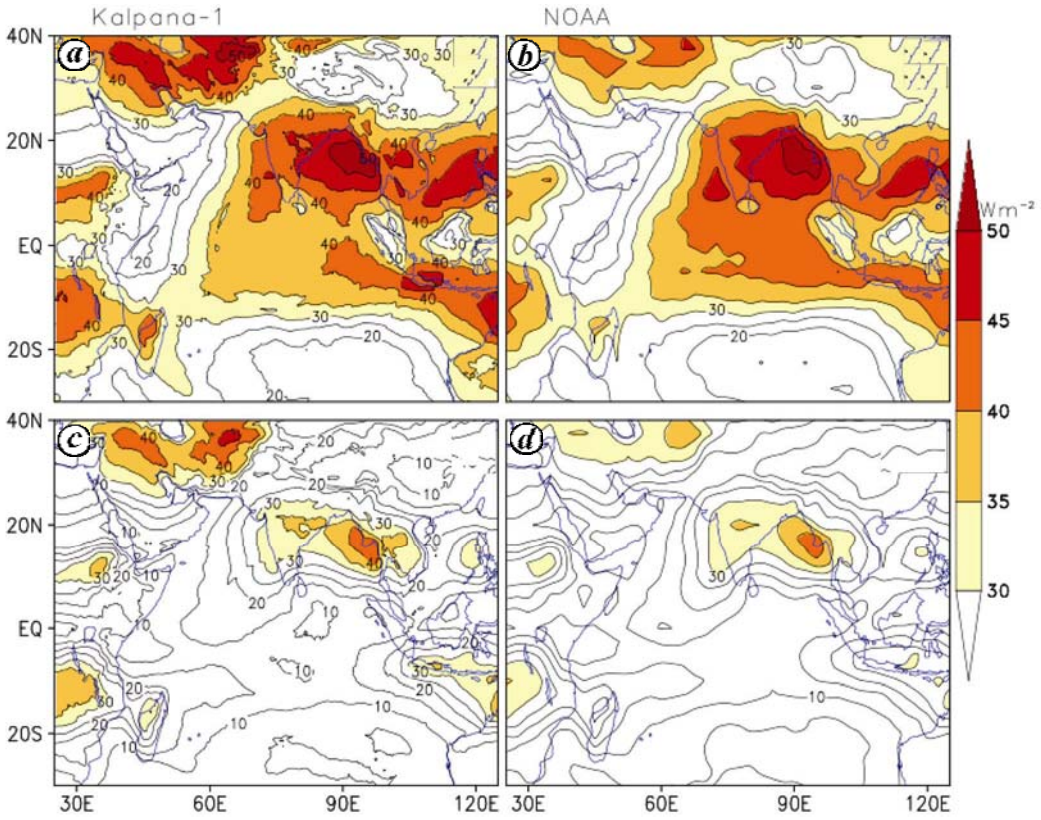

Figure 2. Average standard deviation of daily (***a***) Kalpana-1 and (***b***) NOAA OLR during the periods 2005–2011; ***c*** and ***d***, Average standard deviation of annual cycles obtained from Kalpana-1 and NOAA OLR respectively, during the same period.

continuous (with a gap of nearly ten months during 1978) and routinely available longest data. However, these data are known to have biases in them due to large drift in the orbit of several participating satellites[30].

The variability in the daily OLR from both the datasets was found to be similar, except that the values are slightly more over the equatorial Indian Ocean (Figure 2 *a*, *b*) in the case of NOAA. The strength of the annual cycle (i.e. the average amplitude of the sum of the first three harmonics of the daily data) is similar in both the data. This pattern of standard deviation is similar to that in Figure 1 *c*, implying that the change in OLR over the region is primarily due to presence of monsoonal clouds. The annual cycle (AC) seems to be driving the variability of OLR over the region extending from the Arakan coast, westward up to central and west coast of India and as well as that over the deserts. It is important to note that the standard deviation of Kalpana-1 OLR over the desert is 10–15 Wm^{-2} higher compared to that of NOAA. Thus the large contribution to the variability over the north and equatorial Indian Ocean is due to OLR variations in the intraseasonal to synoptic scales as the AC is weak over that region.

Both the OLR values were compared by making regular bins of 5×5 Wm^{-2} after converting the Kalpana-1 OLR to NOAA grid. Figure 3 shows that the negative bias of around 6 Wm^{-2} in the NOAA OLR compared to Kalpana-1 is due to its underestimation of OLR values larger than 300 Wm^{-2}, i.e. mostly in the cloud-free regions or regions having a warm surface. The bias is much higher for regions having OLR values around 350 Wm^{-2}. However, the number of grid locations having such values is less in the dataset. The root mean square difference between both the OLR values is around 16 Wm^{-2}.

Figure 4 depicts the time series of AC component of both OLR separately over some selected region of interest. The period in which the value of AC is less than 240 Wm^{-2} over the region, almost coincides with the wet season over the region. These are the regions where the fluctuations in the OLR are mostly governed by the AC (Figure 2). From Figure 4 it can be reiterated that the slightly low value of NOAA OLR is due to suppression of AC in the dataset over the regions with less frequent cloud cover. Thus NOAA OLR seems to be negatively biased over the arid and semi-arid land surfaces as well as over the warm, humid oceans[33]. The plots showing difference between the two dataset (figures not shown) revealed that the NOAA OLR values have negative bias over the entire Indian Ocean as well as over the desert regions, particularly during summer months. We are also

validating the Kalpana-1 OLR with the top-of-the-atmosphere longwave flux data available from ScaRaB on-board *Megha-Tropiques* satellite.

Diurnal variations

Seasonal mean of the OLR at every synoptic hour was obtained from the three hourly OLR obtained from Kalpana-1 VHRR radiances. This was further subjected to Fourier transform to find the amplitude and phase angle of the diurnal cycle in terms of local solar time (LST). Figure 5 shows the same for various seasons. The amplitude of the diurnal variation is largest over the land surfaces, especially over the arid regions, approaching as high as 55 Wm^{-2} during monsoon season (June–September), i.e. almost equal to the variability due to seasonal change (Figures 2 *c* and 4). The diurnal signal is always high over the deserts. The seasonal change in diurnal variation is due to fluctuations in cloud cover associated with migration of the intertropical convergence zone over the region, with largest change over the Indian mainland. Over the ocean the amplitude of the diurnal cycle is small, generally less than 5 Wm^{-2} with little seasonal change, except over the Bay of Bengal, where amplitude of the variation is slightly high (around 8 Wm^{-2}) during the wet season. The values are also slightly high over southern Indian Ocean during summer. The oceanic region surrounding the maritime continents has large amplitude of diurnal change similar to the nearby continents. It can be observed that the diurnal variation in OLR over the eastern parts of China is maritime in nature during the boreal summer (Figure 5 *b* and *c*).

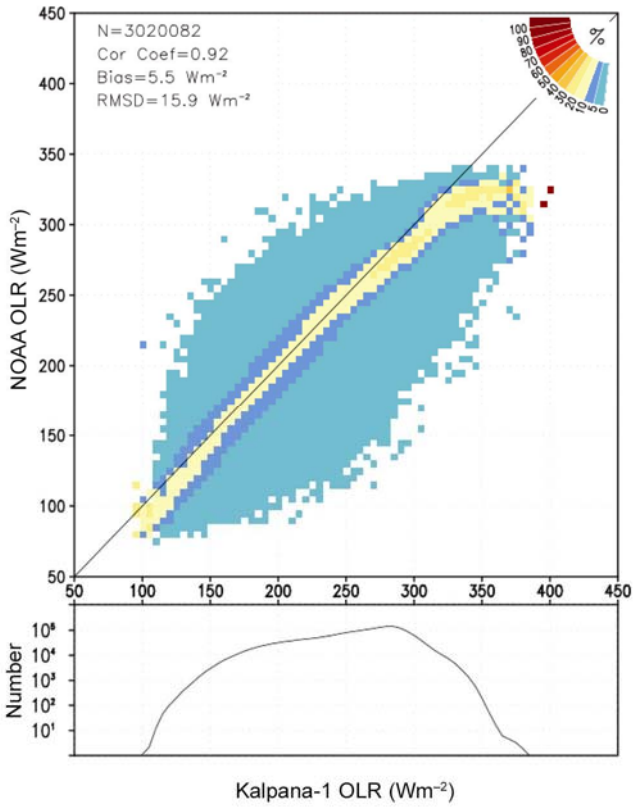

Figure 3. (Upper panel) Percentage of Kalpana-1 and NOAA OLR matched in regular bins of 5 Wm^{-2}. (Lower panel) The number of values in each bin. Daily averaged OLR for the period May 2004–June 2012 was considered for comparison.

The peak in the diurnal amplitude over the southern Bay of Bengal and equatorial Indian Ocean is generally during midnight to sunrise hours during monsoon and post-monsoon seasons, which might have an association with cloud formation. Since the peak in amplitude of diurnal variation of rainfall is between late night and early morning in those regions[34]. The eastern part of central India, i.e. the core monsoon zone shows peaks during monsoon months around 9 LST. OLR values less than 240 Wm^{-2} over a location is generally associated with deep convection or deep clouds.

The frequency of occurrence of OLR with values less than this threshold during monsoon season found to be more than 50% over such region at which average OLR is less than 240 Wm^{-2} (Figure 1 *c*). The frequency of OLR less than a threshold value of 240 Wm^{-2} was calculated for 00–21 LST at three hourly intervals for the monsoon season (JJAS). The average frequency of OLR having values less than 240 Wm^{-2} during the JJAS months was subtracted from each three hourly frequency. The relative change in this frequency during various hours (in LST) is shown in Figure 6 for the monsoon season. It can be seen from the figure that the deep convection is in a relatively suppressed (active) phase over the Indian subcontinent and more pronounced over the eastern part of central India and peninsular regions during 06–12 LST (18–00 LST). Hence, the OLR escaping to space from this region is at its peak around 09 LST, i.e. just before peak hour of insolation (i.e. local noon), at its peak hours of suppressed phase of high cloud coverage. Whereas over regions having less frequent clouds such as deserts, arid and semi-arid regions, diurnal amplitude OLR peaks around local noon.

Wet and dry spells of monsoon

In order to examine the potential of these data in describing the wet (active) and dry (suppress or break) phases in the monsoon convection, the following analysis was performed. Daily anomaly of OLR (OLRA) was found after subtracting the sum of the annual average and first three harmonics for the individual years from its daily value. The OLRA values within the central India region, i.e. over the domain 17.5–27.5°N, 72.5–87.5°E (Figure 7) were averaged to obtain the daily time series OLRA during monsoon season. This region is generally considered as the core monsoon region in the study of monsoon intraseasonal variations[14,35–37]. The wet (dry) spells are

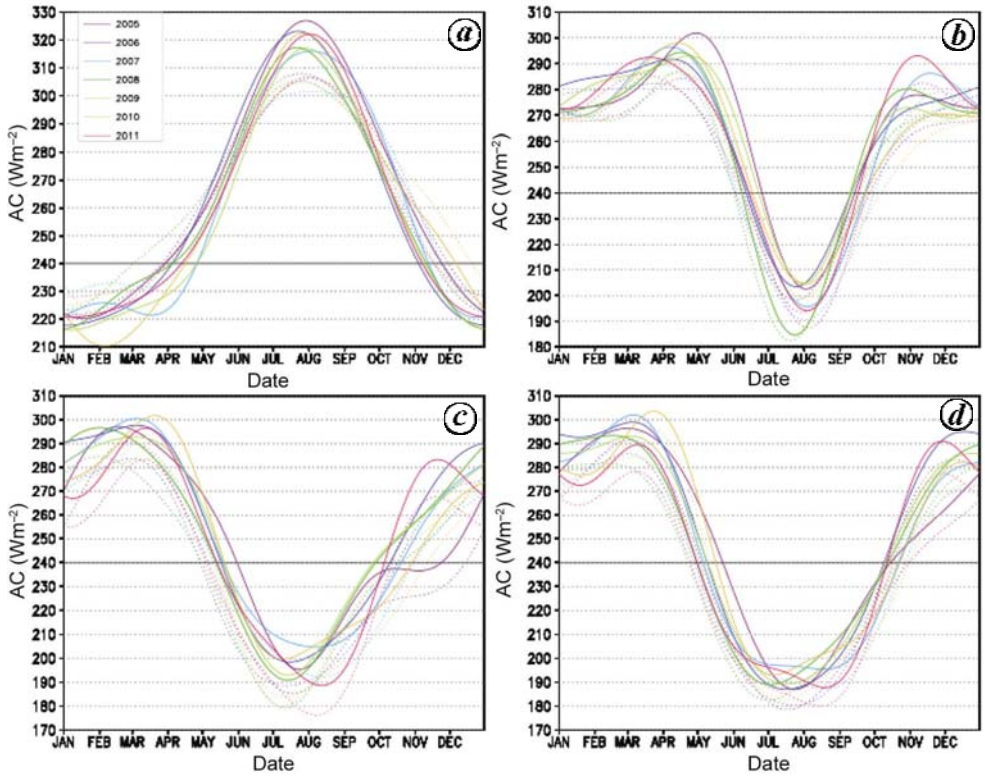

Figure 4. Annual cycles (ACs, i.e. sum of annual average and first three harmonics) of Kalpana-1 (continuous lines) and NOAA (dotted lines) OLR data over few selected regions. (***a***) Desert (30–65°E and 30–40°N), (***b***) Central India (77.5–87.5°E and 17.5–27.5°N), (***c***) Bay of Bengal (84–93°E and 14–16°N) and (***d***) Arakan coast (90–98°E and 14–20°N).

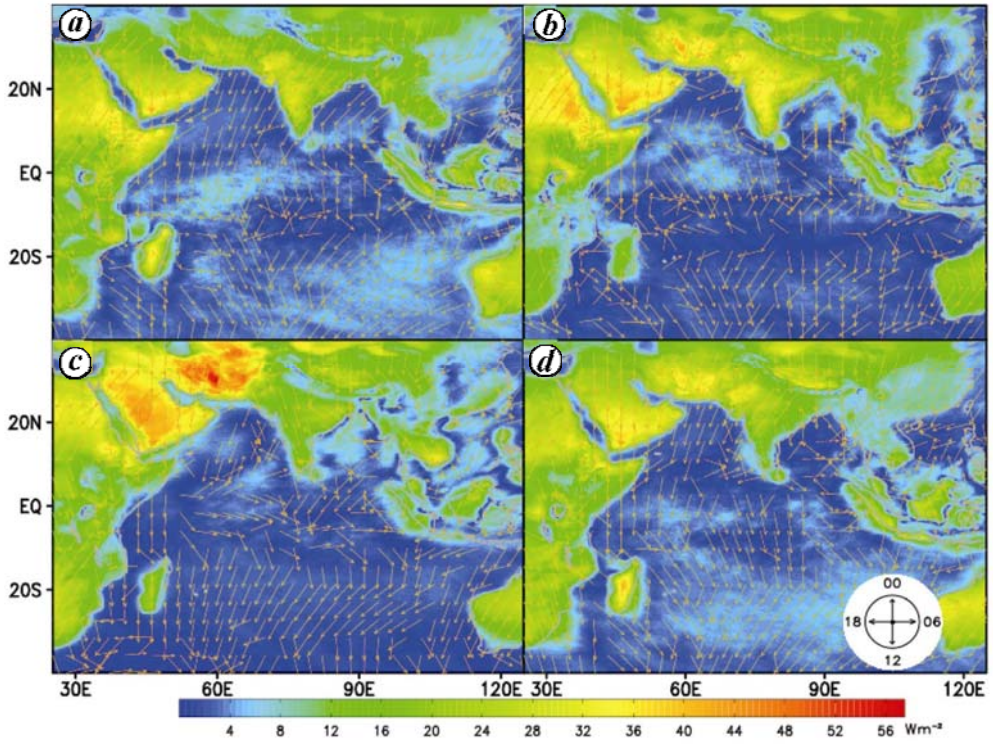

Figure 5. Diurnal variations observed in Kalpana-1 three hourly OLR during various seasons: (***a***) Winter (January–February), (***b***) Pre-monsoon (March–May), (***c***) Monsoon (June–September) and (***d***) Post-monsoon (October–December). Amplitude (Wm^{-2}) is shaded and the phase (in local solar time (LST)) is shown in 24 h clock dial, i.e. arrow pointing northward is for 00 LST peak and southward for 12 LST.

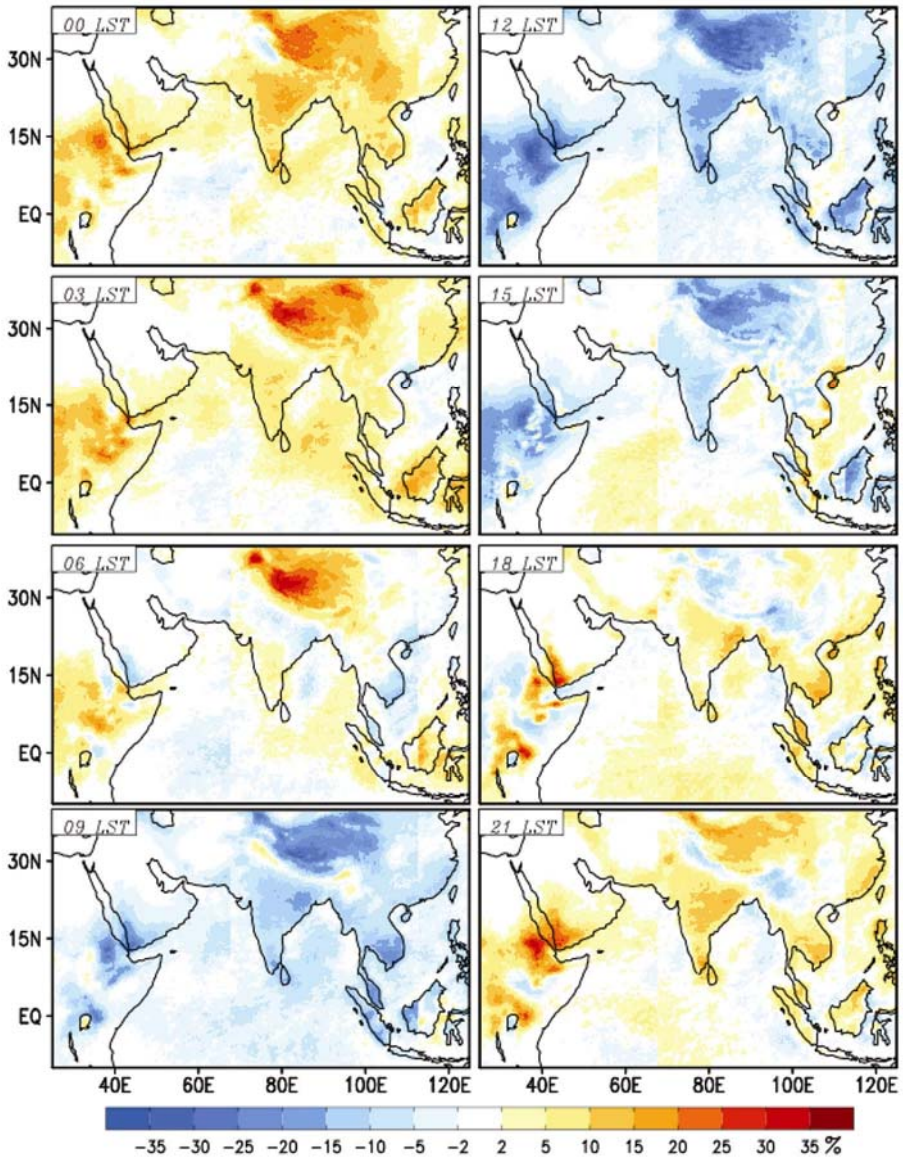

Figure 6. Relative change in frequency of OLR having less than 240 Wm^{-2} threshold during monsoon season (June–September) of 2005–2011.

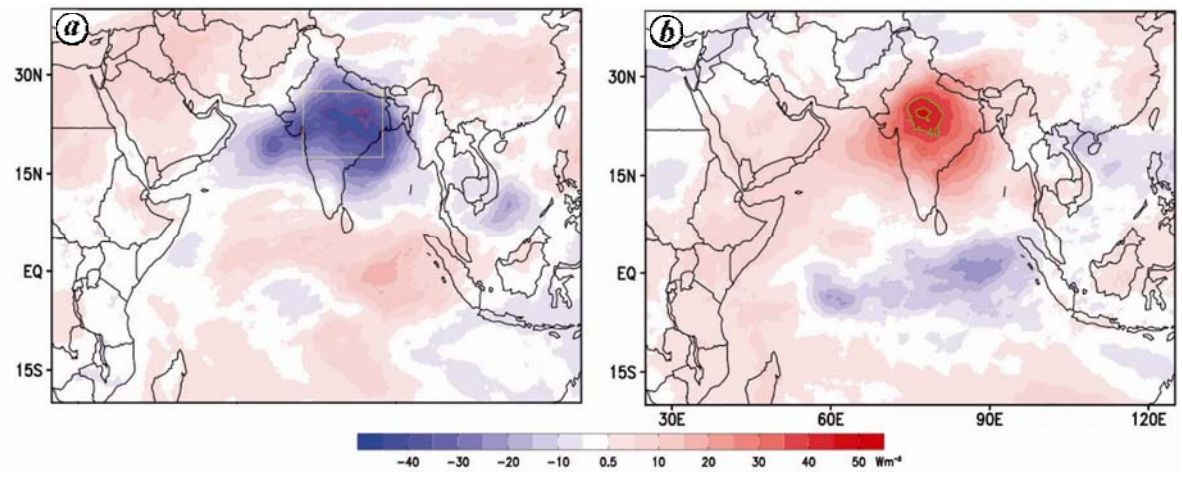

Figure 7. OLR anomalies (OLRA) during active (***a***) and break (***b***) monsoon days for 2005–2011.

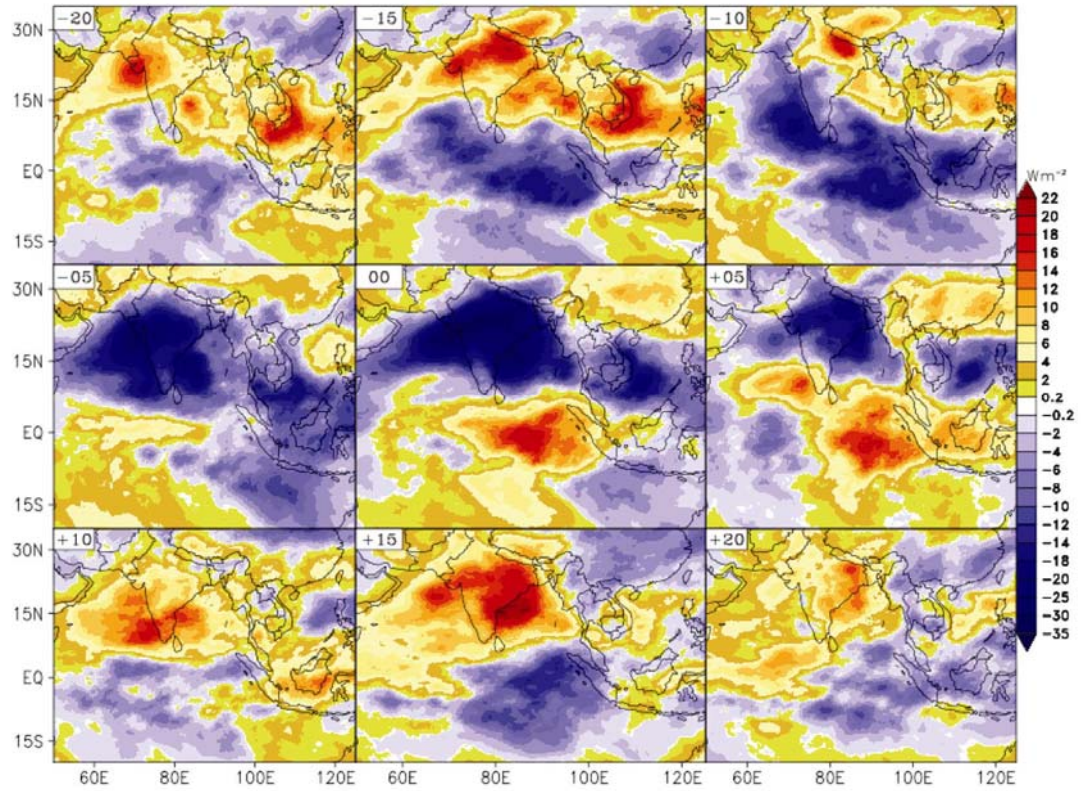

Figure 8. Lag–lead (in days) composite of 20–90 days filtered OLRA with reference to active monsoon days.

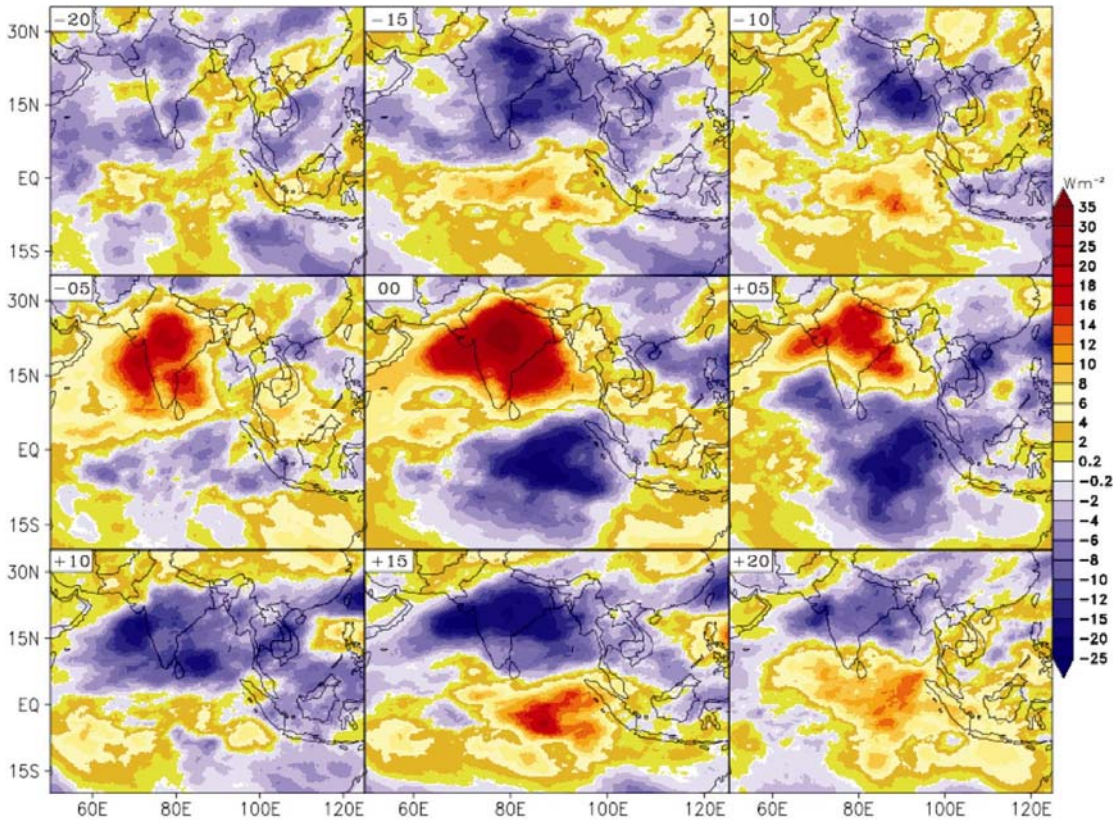

Figure 9. Same as Figure 8 but for break days.

Table 1. Monsoon active and break spells during 2005–2011 obtained from Kalpana-1 and NOAA outgoing longwave radiation

	Active				Break			
	Kalpana-1		NOAA		Kalpana-1		NOAA	
Year	Date	Days	Date	Days	Date	Days	Date	Days
2005	22 June–5 July	14	23 June–4 July	12	1–6 June	5	–	–
	11–18 September	8	8–15 September	8	9–18 June	10	–	–
					7–11 August	5	–	–
					25 August–1 September	8	25 August–1 September	8
2006	1–6 June	6	1–5 June	5	11–18 June	8	11–19 June	9
	27–30 June	4	–	–				
	20–23 September	4	19–23 September	5				
2007	23–27 September	5	22–27 September	6	–	–	–	–
2008	8–19 June	12	5–18 June	14	21–24 August	4	21–24 August	4
	15–20 September	6	15–20 September	6				
2009	27 June–3 July	7	27 June–3 July	7	29 July–4 August	7	29 July–5 August	8
	25–28 August	4	3–7 September	5	12–17 September	6	11–17 September	7
2010	14–19 September	6	14–17 June	4	7–10 August	4	7–10 August	4
			14–18 September	5	24–28 September	5	23–28 September	6
2011	25–29 June	5	25–28 June	4	23–27 July	5	23–27 July	5
	24–17 September	4	14–17 September	4			27–30 September	4
Total (avg)	–	85 (7)	–	85 (7)	–	67 (6)	–	55 (6)

generally associated with the active (break) phase of the monsoon as part of intraseasonal variations. Those spells are identified when the OLRA is below (above) one standard deviation continuously for at least four days. A list of such periods obtained from Kalpana-1 OLRA is given in Table 1. Figure 7 shows the composites of OLRA during active and break days for the period 2005–2011. The figure also shows the generally observed 'quadruple structure' of the convective anomalies associated with active–break cycles[38]. Similarly, active–break (or wet–dry) spells were identified from the NOAA OLRA for these years (Table 1). It is interesting to note that the active–break spells identified from both the datasets match well, except on a few occasions. The average life of an active (break) period identified from Kalpana-1 as well as from NOAA OLR is 7 (6) days.

The time series of average OLRA over central India was further filtered using the Lanczos filter[39] to retain the variations having periodicities in the spectral band of 20–90 days (intra-seasonal or Madden–Julian scale)[40]. Using the above-mentioned criteria the peak days of active/break spells in the monsoon were identified. The lag–lead maps of active–break days in monsoon obtained from Kalpana-1 OLR were prepared with reference to these peak days; (Figures 8 and 9). The plot clearly shows the general evolution of active–break phases of the monsoon convection. The composite structure of the OLR anomalies shows the observed quadruple structure in the spatial pattern in the convective organization. It also shows the general revival of active (break) phases of convection with the northward movement of active (suppressed) convective bands[14,35–40] and with periodicities in the intraseasonal timescales. The northward movement is more pronounced along the eastern Arabian sea adjacent to the west coast of India, which can be seen from Figures 8 and 9.

Summary and conclusion

Three hourly OLR for the period May 2004–June 2012 were estimated over the Indian region (i.e. 40°S–40°N, 25–125°E) from the IR window and WV channel radiances measured by VHRR on-board the Kalpana-1 satellite. The data are relatively better in quality compared to those from polar orbiting NOAA satellites having less frequent sampling, particularly over the warm, humid oceans, semi-arid or arid regions, where NOAA seems to be negatively biased. The active–break periods in the Indian summer monsoon picked up by both data match well. The three hourly OLR estimated from Kalpana-1 VHRR shows that the amplitude of the diurnal variations over the continents is more pronounced compared to that over the oceanic areas in the analysis domain. The OLR estimated from Kalpana-1 will be useful for radiation budgets, monitoring monsoon activity and long term climate.

1. Suomi, V. E., The radiation balance of the earth from a satellite. *Ann. Int. Geophys. Year*, 1957, **6**, 331–340.
2. Jacobwitz, H. W., Smith, H. L., Howell, H. B., Nagle, F. W. and Hickey, J. R., The first 18 months of planetary radiation budget measurements from the Nimbus 6 ERB experiment. *J. Atmos. Sci*., 1979, **36**, 501–507.
3. Gruber, A. and Wintson, J. S., Earth–atmosphere radiative heating based on NOAA scanning radiometer measurements. *Bull. Am. Meteorol. Soc*., 1978, **59**, 1970–1973.

4. Ohring, G. and Gruber, A., Satellite radiation observations and climate theory. *Adv. Geophys*., 1983, **24**, 237–304.
5. Lau, K. M. and Chan, P. H., Short-term climate variability and atmospheric teleconnections from satellite-observed outgoing longwave radiation, Part I: Simultaneous relationships. *J. Atmos. Sci*., 1983, **40**, 2735–2750.
6. Lau, K. M. and Chan, P. H., Short-term climate variability and atmospheric teleconnections from satellite-observed outgoing longwave radiation, Part II: Lagged correlations. *J. Atmos. Sci*., 1983, **40**, 2751–2767.
7. Ardanuy, P. E. and Kyle, H. L., El Niño and outgoing longwave radiation observations from Nimbus-7 ERB. *Mon. Weather Rev*., 1986, **114**, 415–433.
8. Ramanathan, V., Cess, R. D., Harrison, E. F., Minnis, P., Barkstrom, B. R., Ahmad, E. and Hartmann, D., Cloud-radiative forcing and climate: results from the earth radiation budget experiment. *Science*, 1989, **243**, 57–62.
9. Ramanathan, V., The role of earth radiation budget studies in climate and general circulation research. *J. Geophys. Res. D*, 1987, **92**, 4075–4095.
10. Kiehl, J. T. and Ramanathan, V., Comparison of cloud forcing derived from the earth radiation budget experiment with that simulated by the NCAR community climate model. *J. Geophys. Res*., 1990, **95**, 11679–11698.
11. Wild, M., Short-wave and long-wave surface radiation budgets in GCMs: a review based on the IPCC-AR4/CMIP3 models. *Tellus A*, 2008, **60**, 932–945.
12. Goswami, B. N. and Ajaya Mohan, R. S., Intra-seasonal oscillations and inter-annual variability of the Indian summer monsoon, *J. Climate*, 2001, **14**, 1180–1198.
13. Goswami, B. N., South Asian monsoon. In *Intraseasonal Variability of the Atmosphere–Ocean Climate System* (eds Lau, W. K. M. and Waliser, D. E.), Praxis, Springer Berlin, 2005, pp. 19–61.
14. Krishnan, R., Zhang, C. and Sugi, M., Dynamics of breaks in the Indian summer monsoons. *J. Atmos. Sci*., 2000, **57**, 1354–1372.
15. Lau, K.-M. and Chan, P. H., Aspects of the 40–50 day oscillation during the northern summer as inferred from outgoing longwave radiation. *Mon. Weather. Rev*., 1986, **114**, 1354–1367.
16. Hendon, H. H. and Liebmann, B., The life cycle of the Madden–Julian oscillation. *J. Atmos. Sci*., 1994, **51**, 2225–2237.
17. Kiladis, G. N., Meehl, G. A. and Weickmann, K. M., Larger-scale circulation associated with westerly wind bursts and deep convection over the western equatorial pacific. *J. Geophys. Res. D*, 1994, **99**, 18527–18544.
18. Wheller, M. and Kiladis, G. N., Convectively coupled equatorial waves: analysis of clouds and temperature in the wave-number–frequency domain. *J. Atmos. Sci*., 1999, **54**, 374–399.
19. Wheller, M., Kiladis, G. N. and Webseter, P. J., Large-scale dynamical fields associated with convectively coupled equatorial waves. *J. Atmos. Sci*., 2000, **57**, 613–640.
20. Kemball-Cook, S. R. and Weare, B. C., The onset of convection in the Madden–Julian oscillation. *J. Climate*, 2001, **14**, 780–793.
21. Liebmann, B., Marengo, J. A., Glick, J. D., Kousky, V. E., Wainer, I. C. and Massambani, O., A comparison of rainfall, outgoing longwave radiation, and divergence over the Amazon basin. *J. Climate*, 1998, **11**, 2898–2909.
22. Xie, P. and Arkin, P. A., Global monthly precipitation estimates from satellite-observed outgoing longwave radiation. *J. Climate*, 1998, **11**, 137–164.
23. Kaila, V. K. *et al.*, METSAT – a unique mission for weather and climate. *Curr. Sci*., 2002, **9**, 1081–1088.
24. Singh, R., Pal, P. K. and Joshi, P. C., Assimilation of Kalpana very high resolution radiometer water vapour channel radiances into a mesoscale model. *J. Geophys. Res.*, 2010, **115**, D18124.
25. Ohring, G., Gruber, A. and Ellingson, R., Satellite determinations of the relationship between total longwave radiation flux and infrared window radiance. *J. Climate Appl. Meteorol.*, 1984, **23**, 416–425.
26. Gruber, A. and Krueger, A. F., The status of the NOAA outgoing longwave radiation data set. *Bull. Am. Meteorol. Soc*., 1984, **65**, 958–962.
27. Liebmann, B. and Smith, C. A., Description of a complete (interpolated) outgoing longwave radiation dataset. *Bull. Am. Meteorol. Soc*., 1996, **77**, 1275–1277.
28. Rao, A. V. R. K., Kelkar, R. R. and Arkin, P. A., Estimation of precipitation and outgoing longwave radiation from INSAT-1B radiance data. *Mausam*, 1989, **40**, 123–140.
29. Ellingson, R. G., Lee, H. T., Yanuk, D. J. and Gruber, A., A validation of a technique for estimating outgoing longwave radiation from HIRS radiances observations. *J. Atmos. Ocean. Technol.*, 1994, **11**, 357–365.
30. Lucas, L. E., Waliser, D. E., Xie, P., Janowiak, J. E. and Liebmann, B., Estimating the satellite equatorial crossing time biases in the daily, global outgoing longwave radiation dataset. *J. Climate*, 2001, **14**, 2583–2605.
31. Singh, R., Thapliyal, P. K., Kishtawal, C. M., Pal, P. K. and Joshi, P. C., A new technique for estimating outgoing longwave radiation using infrared window and water vapour radiances from Kalpana very high resolution radiometer. *Geophys. Res. Lett.*, 2007, **34**, L238815.
32. Evenden, G. I., Cartographic projection procedures for the UNIX environment – a user's manual. United States Department of the Interior Geological Survey, 1990, pp. 1–68; http://www.remotesening.org/proj
33. Schmetz, J., and Liu, Q., Outgoing longwave radiation and its diurnal variation at regional scales derived from meteosat. *J. Geophys. Res. D*, 1988, **93**, 11192–11204.
34. Sorooshain, S., Gao, X., Hsu, K., Maddox, R. A., Hong, Y., Gupta, H. V. and Imam, B., Diurnal variability of tropical rainfall retrieved from combined GOES and TRMM satellite information. *J. Climate*, 2002, **15**, 983–1001.
35. Joseph, S., Sahai, A. K. and Goswami, B. N., Eastward propagating MJO during boreal summer and Indian monsoon droughts. *Climate Dyn.*, 2009, **32**, 1139–1153.
36. Rajeevan, M., Bhate, J., Kale, J. D. and Lal, B., High resolution daily gridded rainfall data for the Indian region: analysis of break and active monsoon spells. *Curr. Sci*., 2006, **91**, 296–306.
37. Rajeevan, M., Gadgil, S. and Bhate, J., Active and break spells of the Indian summer monsoon. *J. Earth Syst. Sci*., 2010, **119**, 229–247.
38. Annamalai, H., and Slingo, J. M., Active/break cycles: diagnosis of the intraseasonal variability of the Asian summer monsoon. *Climate Dyn.*, 2001, **18**, 85–102.
39. Duchon, C. E., Lanczos filtering in one and two dimensions. *J. Appl. Meteorol*., 1979, **18**, 1016–1022.
40. Madden, R. A. and Julian, P. R., Observations of the 40–50-day tropical oscillation – a review. *Mon. Weather Rev.*, 1994, **122**, 814–837.

ACKNOWLEDGEMENTS. Indian Institute of Tropical Meteorology and India Meteorological Department are fully funded by the Ministry of Earth Sciences, Government of India. Kalpana-1 images (level 1B data) for the period September 2010–2012 used in this work were kindly provided by MOSDAC (ISRO). Interpolated OLR data were provided by the NOAA/OAR/ESRL PSD, Boulder, Colorado, USA, from their website http://www.esrl.noaa.gov/psd/. We thank two anonymous reviewers for their constructive comments, which helped improve the manuscript.

Received 30 September 2012; revised accepted 16 July 2013